ACS APPLIED MATERIALS & INTERFACES

Research Article

www.acsami.org

Near-Infrared Fluorescent Semiconducting Polymer Dots with High Brightness and Pronounced Effect of Positioning Alkyl Chains on the Comonomers

Chuan-Pin Chen, Ya-Chi Huang, Sz-Yu Liou, Pei-Jing Wu, Shih-Yu Kuo, and Yang-Hsiang Chan*

Department of Chemistry, National Sun Yat-sen University, 70 Lien Hai Road, Kaohsiung, Taiwan 80424

Supporting Information

ABSTRACT: In recent years, semiconducting polymer dots (Pdots) have emerged as a novel class of extraordinarily bright fluorescent probes with burgeoning applications in bioimaging and sensing. While the desire for near-infrared (NIR)-emitting agents for in vivo biological applications increases drastically, the direct synthesis of semiconducting polymers that can form Pdots with ultrahigh fluorescence brightness is extremely lacking due to the severe aggregation-caused quenching of the NIR chromophores in Pdots. Here we describe the synthesis of dithienylbenzoselenadiazole (DBS)-based NIR-fluorescing Pdots with ultrahigh brightness and excellent photostability. More importantly, the fluorescence quantum yields of these Pdots could be effectively increased by the introduction of long alkyl chains into the thiophene rings of DBS to significantly inhibit the aggregation-caused emission quenching. Additionally, these new series of DBS-based Pdots can be excited by a commonly used 488 nm laser and show a fluorescence quantum yield as high as 36% with a Stokes shift larger than 200 nm. Single-particle analysis indicates that the per-particle brightness of the Pdots is at least 2 times higher than that of the commercial quantum dot (Qdot705) under identical laser excitation and acquisition conditions. We also functionalized the Pdots with carboxylic acid groups and then linked biomolecules to Pdot surfaces to demonstrate their capability for specific cellular labeling without any noticeable nonspecific binding. Our results suggest that these DBS-based NIR-fluorescing Pdots will be very practical in various biological imaging and analytical applications.

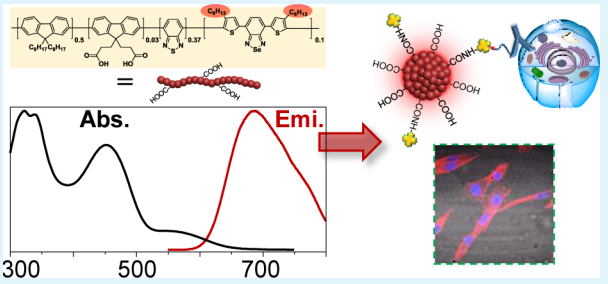

KEYWORDS: *dithienylbenzoselenadiazole, semiconducting polymer dots, near-infrared fluorescence, specific cellular labeling, conjugated polymers, conjugated polymer nanoparticles*

INTRODUCTION

Recently, great efforts have been made toward the investigation of biological processes at the single-cell level in a live organism, including the measurement of single-cell activity, gene regulation, DNA repair mechanisms, and diagnosis of disease.[1−3] Accordingly, the exploration of optical monitoring at subcellular scales has become a pressing issue. Among the various imaging techniques of biological systems, fluorescence microscopy is, by far, one of the most powerful cellular analysis tools because of its high signal-to-noise ratio, excellent spatial and temporal resolution, and noninvasive nature. Moreover, the recent advances in fluorescence image-guided surgery[4] and its first in-human investigation in staging and cytoreductive surgery for ovarian cancer[5] has demonstrated the utilities of fluorescence imaging techniques and greatly emphasized the importance for choosing proper fluorescent probes. Recently, enormous efforts have been devoted to developing new fluorescent agents with fluorescence wavelengths in the near-infrared (NIR) region (650−900 nm) for bioimaging and clinical diagnosis owing to their low photodamage to biological species, low interference from autofluorescence in biological tissues, smaller scattering in turbid media, and longer penetration in tissues.[6,7]

Several types of NIR fluorescent markers have been explored such as small organic dyes and nanoparticle-based probes. Although conventional organic dyes are the most prevalent fluorescent probes, nanoparticle-based fluorescent probes (e.g., dye-doped silica/polymer nanoparticles or quantum dots)[8−17] provide numerous prominent merits over small organic fluorescent dyes including improved photostability, higher fluorescence brightness, good water solubility, and large Stokes shift, which have demonstrated their usefulness in biological imaging with high sensitivity, long-term in vivo imaging, and high-throughput analysis. Nevertheless, many concerns such as leakage of the encapsulated dyes from the silica or polymer matrices[18,19] and potential release of the inorganic element (e.g., Cd)[12,20,21] might largely hinder their physiological use and clinical implementation. In recent years, upconverting and NIR fluorescent rare earth nanomaterials have been extensively

Received: September 25, 2014
Accepted: November 14, 2014
Published: November 14, 2014

investigated due to their excellent optical characteristics.[22] However, their relatively low quantum yields and small absorption cross section may lead to low per-particle fluorescence brightness. Consequently, the design of NIR-emitting nanoparticle-based materials with high fluorescence brightness, excellent photostability, and good biocompatibility is highly desirable.

Semiconducting polymer dots (Pdots) have recently become as a new type of fluorescent probes with superior fluorescence brightness, excellent photostability, large radiative rate, easy surface functionalization, and minimal cytotoxicity,[23−32] which have rendered them very practical for various in vitro and in vivo applications.[6,33−46] Despite the enormous progress, the synthesis of suitable NIR fluorescent semiconducting polymers for generating Pdots is still a significant challenge, partially because of the rigid and flat extended π-conjugated skeletons of NIR polymers that result in the serious self-quenching upon condensation into a Pdot form.[47−51] Accordingly, there have been several approaches developed to address the aforementioned challenge. For example, Chiu's group embedded the NIR dye, silicon 2,3-naphthalocyanine bis(trihexylsilyloxide), into the matrix of poly(9,9-dioctylfluorene-*co*-benzothiadiazole) (PFBT) Pdots.[6] The efficient energy transfer from the PFBT matrix to the NIR dyes has greatly increased the fluorescence brightness of the NIR dyes. Similarly, Zhang et al. blended more than three kinds of conjugated polymers together with the optimized molar ratio inside a Pdot where the NIR emission could be accomplished via cascade Förster resonance energy transfer (FRET).[52] In these two studies, however, the potential leaching of the encapsulated dyes/polymers remains an important concern due to the lack of stable covalent linkages between the doped molecules and the Pdot matrix, which would greatly influence the photophysical properties of Pdots.[40] Very recently, our group has successfully created a facile and scalable approach to overcome the leaching issue by enclosing the NIR dye doped Pdots with polydiacetylenes and at the same time the carboxyl-functionalized polydiacetylenes could be further conjugated with streptavidin for specific cellular targeting.[53]

Although the aforementioned approaches can create NIR-emitting Pdots, most of the NIR chromophores still suffer from the issue of aggregation-caused quenching due to their strong $\pi-\pi$ stacking intramolecular interactions upon condensation into a Pdot form. As a trade-off, therefore, only a small molar fraction of NIR chromophores (usually <3%) can be doped into the Pdot matrix in an effort to achieve a high fluorescence quantum yield. This might potentially affect the photostability of Pdots once a strong laser excitation is required during the experiments (e.g., single-molecule imaging), where rapid photobleaching of NIR emitters usually occurs. Additionally, the direct incorporation of NIR-fluorescing moieties into polymer backbones remains the premier option owing to the robust covalent bonds that can prevent the potential dye leakage and the amplified energy transfer inside conjugated polymers that can be exploited for various bioimaging and sensing applications. To address the aforementioned challenges, we report here the design and synthesis of semiconducting polymers containing dithienylbenzoselenadiazole (DBS) monomers for generating a new class of NIR fluorescent Pdots with ultrahigh fluorescence brightness. First, we systematically tuned the molar ratios of DBS in the copolymers in order to study the influence of copolymer composition on the optical performance of the corresponding Pdots. We then introduced the long alkyl chains on the thiophene moieties of DBS units and then investigated the effect of alkyl position (either in the 3-/inner position or 4-/outer position of both thiophene rings) on the optical properties of the resulting Pdots. More importantly, we directly fabricated the side chains of the semiconducting polymers with carboxylic acid functional groups, making Pdots applicable to further functionalization for specific cellular labeling or sensing applications. Herein we have carried out biomolecular conjugation to demonstrate their specific cellular targeting ability by use of fluorescence imaging and flow cytometry experiments. We believe this work has shown the promising applicability of these DBS-based NIR-fluorescent Pdots in a wide range of biological imaging and diagnostic assays.

RESULTS AND DISCUSSION

Our aim was to synthesize bright NIR fluorescent Pdots that based on DBS emitters and study how the alkyl substitutions on the thiophene rings affect their fluorescence. Functionalization of Pdots was achieved by covalently linking carboxylate functional groups to the fluorene monomers in the polymer backbone so that they could be tagged with biological molecules for specific cellular targeting applications.

Design and Synthesis of DBS-Containing Copolymers with NIR Fluorescence. In an effort to design NIR-emitting polymers, we herein employed the donor−acceptor strategy by incorporating fluorene derivatives (donor) and NIR-emissive DBS monomers (acceptor) into the polymer backbone. To date, however, almost all of the fluorescence quantum yields of the copolymers drop drastically as the concentrations of the NIR-emitting units are increased. This serious aggregation-caused quenching phenomenon leads to the fact that only a small molar ratio (usually <3%) of NIR units can be incorporated with the comonomers (fluorene derivatives are used in most cases) in order to maintain a high fluorescence quantum yield. Accordingly, the resulting copolymers containing a small fraction of NIR monomers can be excited only in the ultraviolet region (350−410 nm) due to the dominant absorption of fluorene moieties, which is a serious disadvantage for many biological applications. To circumvent this problem, we introduced an intermediate donor, benzothiadiazole (BT), into the copolymer backbone to achieve efficient intraparticle energy transfer from this BT donor to the NIR chromophore (i.e., DBS monomer) because of the substantial spectral overlap between the emission spectrum of the BT donor (λ_{max}^{em} = 540 nm)[32] and the absorption spectrum of the NIR-emissive DBS ($\lambda_{max}^{abs} \sim$ 550 nm, *vide infra*). This design allows the Pdots to be excited by the generally used excitation laser at 488 nm. As such, we first synthesized DBS monomer and then polymerized with the BT donor and the fluorene derivative via palladium-catalyzed Suzuki coupling to form a copolymer **PFBT-DBSX** (Figure 1). We also varied the molar ratio DBS monomers (1−50%) to investigate the influence of various copolymer compositions on the optical properties of the resulting Pdots. We further modified the structure of DBS unit by incorporating the long alkyl chains on its thiophene rings (**PFBT-DBSOC$_6$X** and **PFBT-DBSIC$_6$X**) to tune the Pdot emission color and the fluorescence quantum yield. Similarly, the molar ratios of DBS-based monomers were systematically tuned to study their effects on the Pdot optical performance.

The general synthetic routes toward the monomers and copolymers are outlined in Scheme 1. Monomer **8a** and **8b** were synthesized by Stille coupling from monomer **3** and

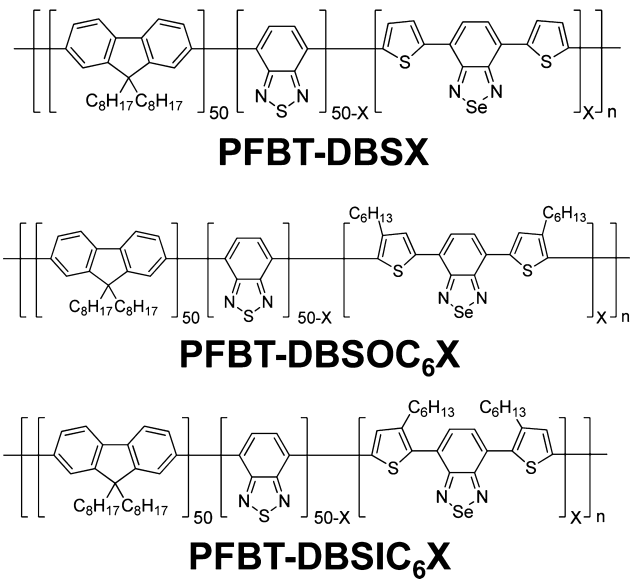

Figure 1. Chemical structures of DBS-containing polymers. X = 1, 4, 10, 33, or 50.

monomer **4**/**6**, while monomer **8c** was produced via Suzuki coupling, followed by the bromination by use of NBS. DBS-containing conjugated copolymers (**PFBT-DBSX**, **PFBT-DBSOC$_6$X**, and **PFBT-DBSIC$_6$X**) of different compositions were then prepared from monomer **9**, BT donor, and monomer **8a**/**8b**/**8c** via Suzuki polycondensation. For polymer **PFBT-DBSX**, the molar percentage of fluorene was fixed at 50%, while the comonomer molar ratios of BT to DBS were 0.49:0.01, 0.46:0.04, 0.40:0.10, 0.17:0.33, and 0.00:0.50, respectively; and the corresponding copolymers were denominated as **PFBT-DBS1**, **PFBT-DBS4**, **PFBT-DBS10**, **PFBT-DBS33**, and **PFBT-DBS50**, respectively. The same denomination rule was also applied to **PFBT-DBSOC$_6$X** and **PFBT-DBSIC$_6$X** polymer series. It should be noted that the molar ratios of DBS showed here represent the feeding ratios because the true molar ratios could not be accurately estimated from ^{1}HNMR spectra, especially for those with low DBS ratios (1% and 4%). For the polymers with higher DBS ratios (>10%), the true molar ratios of DBS could be roughly determined by ^{1}H NMR spectra (see the Supporting Information, PFBT-DBSOC$_6$10 as an example in this case). More importantly, we also directly functionalized the semiconducting polymers with carboxylic acid groups on the side chains of fluorene moieties through robust covalent bonding, which can overcome the leaching issues encountered by the other surface functionalization strategies such as surface encapsulation and polymer coprecipitation methods.[40] For example, carboxyl-functionalized fluorene, monomer **12** (see the Supporting Information for synthetic details) was incorporated into the backbone of **PFBT-DBSOC$_6$10** polymer, followed by the removal of protecting *tert*-butyl groups by use of trifluoroacetic acid to form **PFBT-DBSOC$_6$10-COOH** (Scheme 1). Here we fed only 3% of carboxylic acid groups into the polymer backbones because Chiu's group has previously found that the conjugated polymers with lower density of carboxylic acid side chains (~2%) can form robust and bright Pdots in comparison with those with higher density of carboxylic acid functional groups (>14%).[54] The carboxyl functionalized polymers (e.g., **PFBT-DBSOC$_6$10-COOH**) can be further conjugated with biomolecules for specific cellular labeling.

Optical Properties of DBS-Based Pdots. Scheme 2 illustrates the procedures for the preparation of Pdots (**PFBT-DBSOC$_6$10-COOH** as an example in this scheme). Briefly, semiconducting polymer was first dissolved in tetrahydrofuran (THF) and then rapidly injected into a water solution under vigorous sonication. THF was then removed to form a stable Pdot suspension. The average particle size was determined by dynamic light scattering (DLS) and transmission electron microscopy (TEM) to be ~23 nm in diameter. Figure 2 shows the absorption and fluorescence spectra of DBS-based Pdots of different ratios of BT to DBS. The absorption peaks at 300−400 nm, 400−500 nm, and 500−700 nm are attributed to the fluorene segments, BT units, and DBS derivatives in the copolymers, respectively. The insets in Figure 2A represent the photographs of Pdot solutions containing different molar fractions of DBS in the copolymers (left to right: 1 to 50% DBS monomers). Their corresponding fluorescence emission spectra are shown in Figure 2B. The emission maxima of these Pdots locate from 670 to 760 nm, depending on the molar ratio of DBS derivatives and the position of *n*-hexyl substituents on the thiophene rings. The upper insets in Figure 2B show the photographs of Pdot solutions from 1 to 50% DBS (left to right) under a UV lamp. Table 1 summarizes the photophyical properties of this series of DBS-based Pdots. For the same type of copolymers (e.g., **PFBT-DBSX**), the emission peaks of Pdots were gradually red-shifted with increasing molar ratios of DBS in the copolymers, accompanied by the decreases in the fluorescence quantum yields. This phenomenon was attributed to the aggregation-caused quenching of the DBS chromophores in which the large conjugation system of DBS led to the redshift at the same time. Interestingly, we found that the introduction of the hexyl alkyl chains into the thiophene rings (e.g., **PFBT-DBSOC$_6$X** and **PFBT-DBSIC$_6$X**) could efficiently relieve the extent of aggregation-caused quenching. For example, with the increasing DBS content in the copolymers from 1% to 10%, the fluorescence quantum yields decreased by only 33% and 58% for **PFBT-DBSIC$_6$X** and **PFBT-DBSOC$_6$X** Pdots, respectively, as compared to 90% for **PFBT-DBSX** Pdots. This clearly indicates that the incorporation of long alkyl chains into either the 3- or 4-position of the thiophene rings can efficiently prevent the close packing of DBS monomers and thereby maintains their high quantum yields even at an elevated DBS molar ratio. Having a high percentage of DBS emitters in the Pdots to minimize the influence of photobleaching by the excitation laser is crucial to various applications such as long-term particle tracking measurements or the experiments that require a strong laser excitation for prolonged observation (e.g., single-molecule imaging), in which a steady fluorescence is highly demanded in both cases. We also performed photostability measurements by comparing **PFBT-DBSOC$_6$1** with **PFBT-DBSOC$_6$10** Pdots and further confirmed that higher DBS content possesses improved photostability (Figure S1). By taking advantage of the steric effect from alkyl substitution on thiophene rings, we have successfully obtained ultrabright and photostable NIR fluorescent Pdots with a moderate molar ratio of the DBS emitter (i.e., **PFBT-DBSOC$_6$10**, see below for the measurements of single-particle fluorescence brightness). To see if other types of side chains can have the same influence on the optical performance, we also synthesized long alkoxyl chains and branched-alkyl chains on the thiophene moieties of DBS (Scheme S2). We found that the long alkoxyl chains could further redshift the emission of the Pdots due to their strong electron-donating ability, while the branched-alkyl chains could

Scheme 1. Synthetic Routes of DBS Comonomers and Copolymers

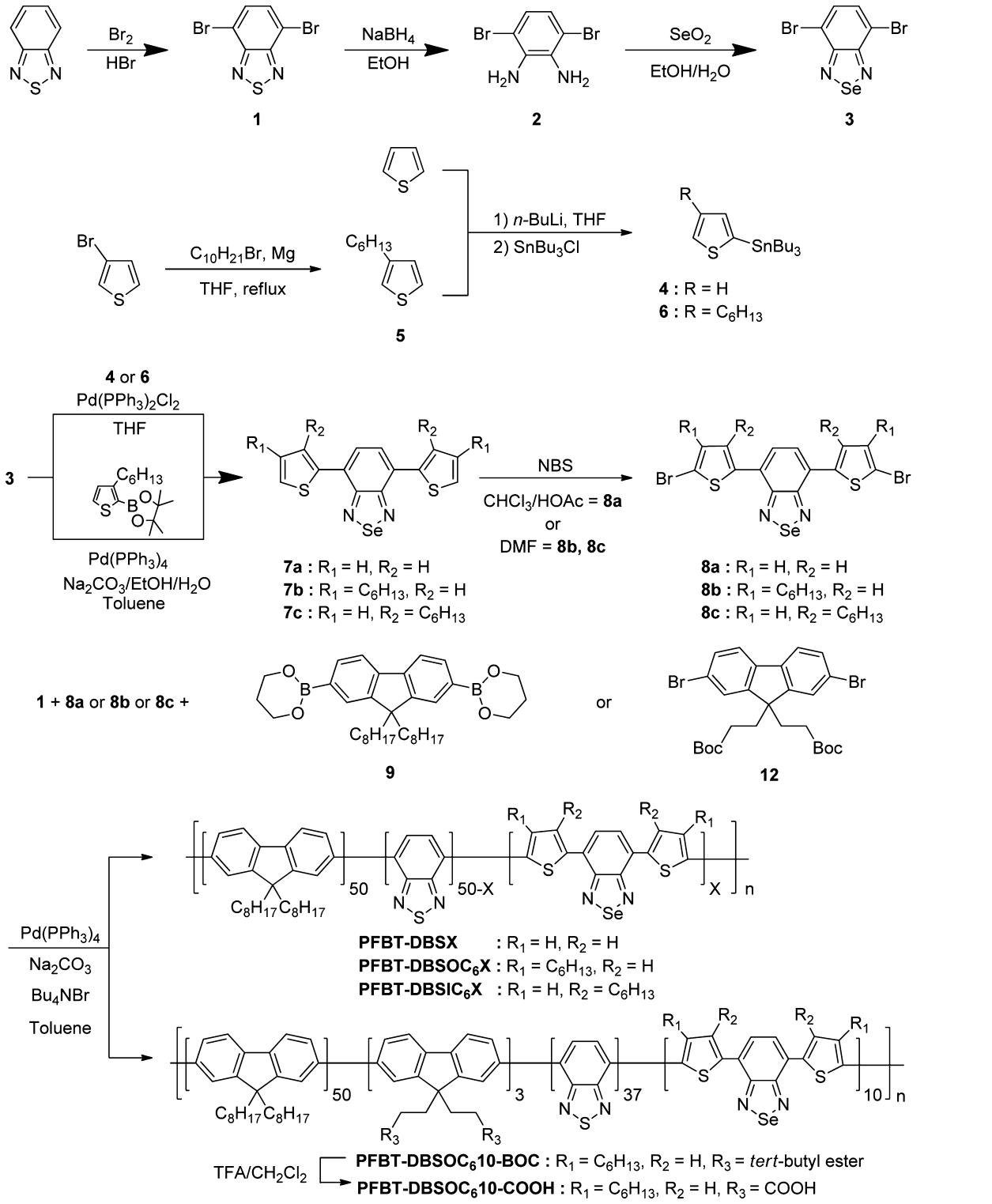

further increase the quantum yield of the Pdots because of their bulky construction. Their optical properties in Pdot form were summarized in Table S1.

We also used a time-correlated single-photon counting module system to determine the fluorescence lifetime (τ) of **PFBT-DBSOC$_6$X** Pdots to be ~2.4 ns (Figure S2). The fluorescence radiative decay rate constant (K_R) and non-radiative rate constant (K_{NR}) containing all possible non-radiative decay pathways can also be estimated from the combination of the following two equations:

$$\Phi = K_R/(K_R + K_{NR}) \quad (1)$$

$$\tau = (K_R + K_{NR})^{-1} \quad (2)$$

Here we take **PFBT-DBSOC$_6$10** Pdots as an example, the **PFBT-DBSOC$_6$10** Pdots exhibit a radiative decay rate of 6.3 ×

Scheme 2. Schematic Illustration of Preparation of Carboxyl-Functionalized DBS-Based Pdots and Subsequent Bioconjugation for Specific Cellular Targeting[a]

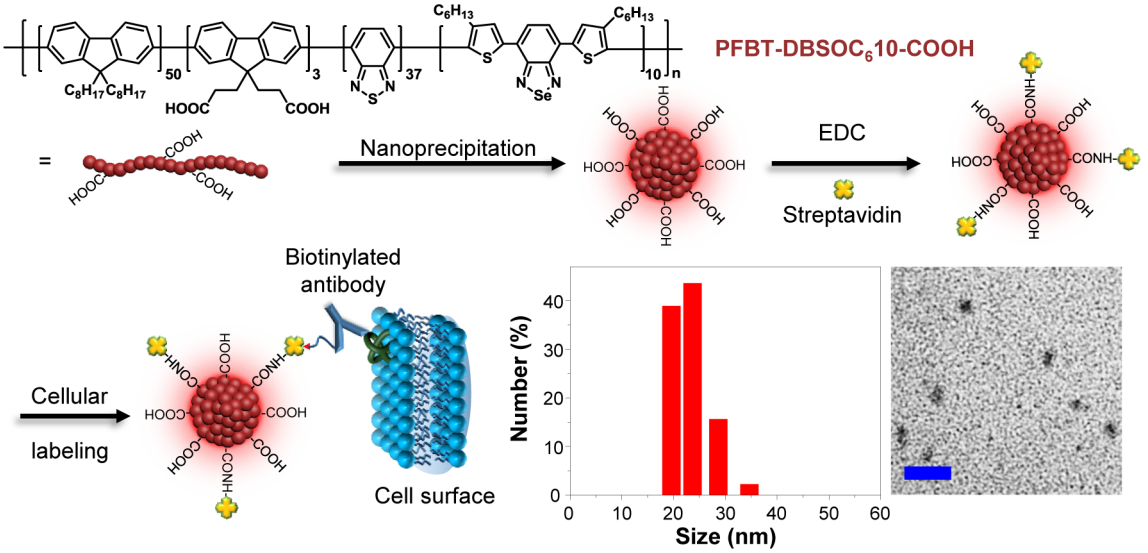

[a]First, semiconducting polymer (**PFBT-DBSOC$_6$10-COOH** as an example in this scheme) were mixed together in THF and then coprecipitated in water under vigorous sonication to form Pdots. The carboxyl-functionalized Pdots were subsequently conjugated to streptavidin via EDC-catalyzed coupling for specific cellular targeting studies. (Left) Hydrodynamic diameters (average diameter was 23 nm) measured by dynamic light scattering and (right) transmission electron microscopy image of Pdots are shown in the right-bottom corner, respectively. Scale bar represents 100 nm.

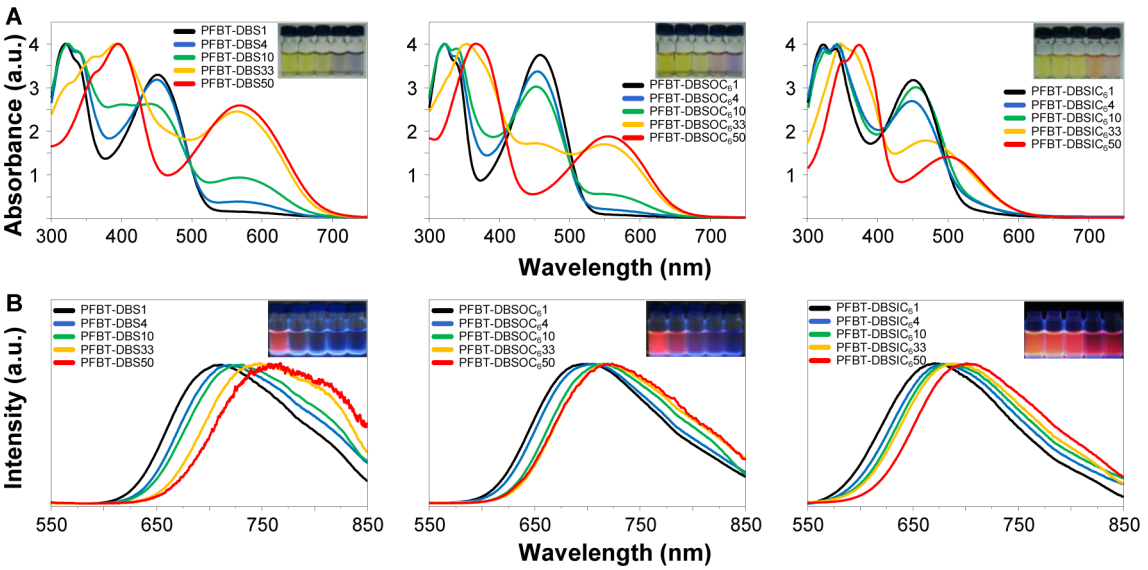

Figure 2. (A) UV−visible spectra of **PFBT-DBSX**, **PFBT-DBSOC$_6$X**, and **PFBT-DBSIC$_6$X** Pdot series in water. The insets in each figures show the photographs of the Pdot solutions (from left to right: 1% to 50% of DBS in sequence). (B) Fluorescence spectra of **PFBT-DBSX**, **PFBT-DBSOC$_6$X**, and **PFBT-DBSIC$_6$X** Pdot series in water. The insets in each figures show their corresponding Pdot solutions under 365 nm UV light (from left to right: 1% to 50% of DBS in sequence).

10^7 s^{-1}, which is comparable to conventional fluorescent dyes and other Pdots reported elsewhere.[23]

Single-Particle Fluorescence Brightness. Single-particle fluorescence brightness is one of the important characteristics of Pdots while applied in bioimaging and sensing. Because the fluorescence brightness can be estimated from the product of the per-particle absorption cross section and the fluorescence quantum yield, it is critical for Pdots to have both the large peak absorption cross section and the high quantum yield in an effort to achieve high fluorescence brightness. Table 2 summarizes the photophysical properties of several DBS-based Pdot suspensions in water in comparison to other water-soluble typical NIR emitting dyes and quantum dots. Here we take copolymers with 10% DBS as examples due to their improved photostability. The peak absorption cross section of single Pdots was calculated from the UV/vis absorbance of known Pdot concentrations, and their absolute fluorescence quantum yields were measured by using an integrating sphere unit. It clearly shows that **PFBT-DBSOC$_6$10** Pdots exhibit the highest fluorescence brightness, which is about 3 orders of magnitude higher than conventional organic dyes or ~1.6 times larger than that of CdSe quantum dots (Qdots705, λ_{max}^{em} = 705 nm, purchased from Invitrogen). Moreover, we specifically compared **PFBT-DBSOC$_6$10** Pdots with Qdots705 nanocryst-

Table 1. Summary of Photophysical Properties of DBS-Based Copolymer Series in Pdot Form in Water (in an Aqueous Solution)

copolymers	λ_{max}^{abs} (nm)[a]	λ_{max}^{em} (nm)[b]	Φ (%)[c]
PFBT-DBS1	320, 452	709	20
PFBT-DBS4	323, 450, 566	719	6
PFBT-DBS10	324, 445, 567	730	2
PFBT-DBS33	394, 568	747	2
PFBT-DBS50	397, 570	760	1
PFBT-DBSOC$_6$1	321, 458	701	36
PFBT-DBSOC$_6$4	322, 453, 543	711	29
PFBT-DBSOC$_6$10	323, 453, 550	715	15
PFBT-DBSOC$_6$33	354, 552	720	3
PFBT-DBSOC$_6$50	367, 557	724	2
PFBT-DBSIC$_6$1	322, 450	672	12
PFBT-DBSIC$_6$4	341, 448	680	11
PFBT-DBSIC$_6$10	342, 455	684	8
PFBT-DBSIC$_6$33	349, 472	690	2
PFBT-DBSIC$_6$50	373, 500	702	2

[a]Absorption maximum. [b]Fluorescence maximum. [c]Quantum yield.

als and found that **PFBT-DBSOC$_6$10** Pdots are calculated to be 2−3 times brighter than Qdots705 probes under 488 nm laser excitation (values are shown in the brackets in Table 2). Experimentally we further performed measurements of single-particle brightness in which the measured average per-particle brightness of **PFBT-DBSOC$_6$10** Pdots (Figure 3B) was indeed ∼2 times higher than that of Qdots705 (Figure 3A) under identical excitation (488 nm) and acquisition conditions, consistent with the calculated results. All of the above results demonstrate that our new series of DBS-based NIR emitting Pdots reported in this work have shown their promising applications in biological imaging and analysis.

Bioconjugation and Specific Cellular Labeling with PFBT-DBSOC$_6$10-COOH Pdots. To demonstrate the applicability of these DBS-based Pdots functionalized with carboxylic acid groups for biological imaging, we performed bioconjugation with streptavidin via 1-ethyl-3-[3-(dimethylamino)propyl]-carbodiimide hydrochloride (EDC)-catalyzed coupling for specific cellular targeting (Scheme 2, **PFBT-DBSOC$_6$10-COOH** as an example in this scheme). Microtubule labeling inside HeLa cells were carried out in which the biotinylated monoclonal anti-α-tubulin antibody and Pdot-streptavidin conjugates were sequentially incubated with the cells. Figure 4A-C shows typical confocal images of Pdot-streptavidin-labeled microtubules in HeLa cells, which indicates that Pdots could be specifically labeled onto subcellular organelles in the

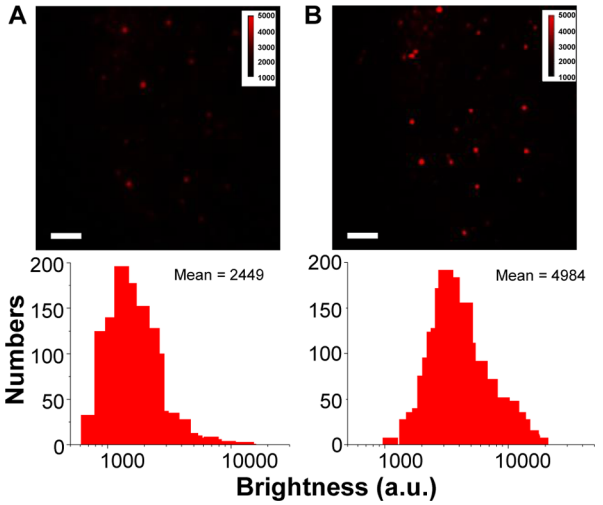

Figure 3. (A) Single-particle fluorescence image of commercial Qdot705 (upper graph) and the corresponding histograms showing the intensity distributions (bottom graph). (B) (A) Single-particle fluorescence image of **PFBT-DBSOC$_6$10** Pdots (upper graph) and the corresponding histograms showing the intensity distributions (bottom graph). Both image were obtained with a 488 nm laser under the same excitation power and identical detection conditions.

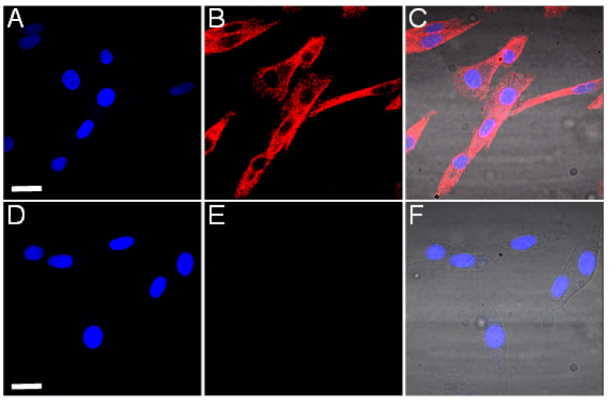

Figure 4. Two-color confocal microscopy images of microtubules in HeLa cells labeled with Pdot-streptavidin conjugates. The blue fluorescence was from nuclear counterstain Hoechst 34580 and the red fluorescence was from Pdot-streptavidin. (A) Image of nucleus. (B) Image of microtubules. (C) The overlay of panels (A) and (B) and the bright-field image. (D-F) Images of negative control samples where cells were incubated with Pdot-streptavidin conjugates but in the absence of biotinylated primary antibody. The scale bars are 20 μm.

Table 2. Photophysical Data Three Types of DBS-Based Pdots in Water Compared with Other Water-Soluble Typical NIR Emitting Dyes

fluorescent probes	λ_{max}^{abs} (nm)	λ_{max}^{em} (nm)	fwhm[e] (nm)	ε_{max} (M^{-1} cm^{-1})	Φ (%)	brightness (ε_{max} x Φ) (M^{-1} cm^{-1})
ATTO740[a]	740	764	43	1.20×10^5	10	1.20×10^6
Cy 5.5[b]	674	694	44	1.95×10^5	23	4.49×10^6
NIR7.0-2[b]	777	798	∼50	1.20×10^5	2.5	3.00×10^5
Qdots705[c]	405 (488)	708	66	$8.30\ (3.50) \times 10^6$	82	$6.81\ (2.87) \times 10^8$
PFBT-DBS10[d]	440	730	153	1.82×10^8	2	3.64×10^8
PFBT-DBSOC$_6$10[d]	455 (488)	712	148	$7.47\ (4.69) \times 10^7$	15	$1.12\ (0.70) \times 10^9$
PFBT-DBSIC$_6$10[d]	455	675	142	6.23×10^7	8	4.98×10^8

[a]Data from ATTO-TEC catalog. [b]Data from C. Bouteiller, G. Clavé, A. Bernardin, B. Chipon, M. Massoneau, P.-Y. Renard, A. Romieu *Bioconjugate Chem.* **2007**, *18*, 1303−1317. [c]Data from Invitrogen (Life Technologies). [d]Pdots in deionized water. [e]Full width at half-maximum.

presence of biotinylated antibody. Figure 4D-F shows the confocal fluorescence images of negative control samples in which no noticeable emission signal from Pdots was observed. These results indicate that this new class of DBS-based Pdots has highly specific labeling activity with minimal nonspecific adsorption.

Additionally, we also carried out flow cytometry experiments where Pdot-streptavidin conjugates were used to label membrane proteins on MCF-7 cells. The cells were sequentially incubated with biotinylated primary antihuman CD326 EpCAM antibody and Pdot-streptavidin conjugates. As shown in Figure 5A, the Pdot-streptavidin probes could be effectively

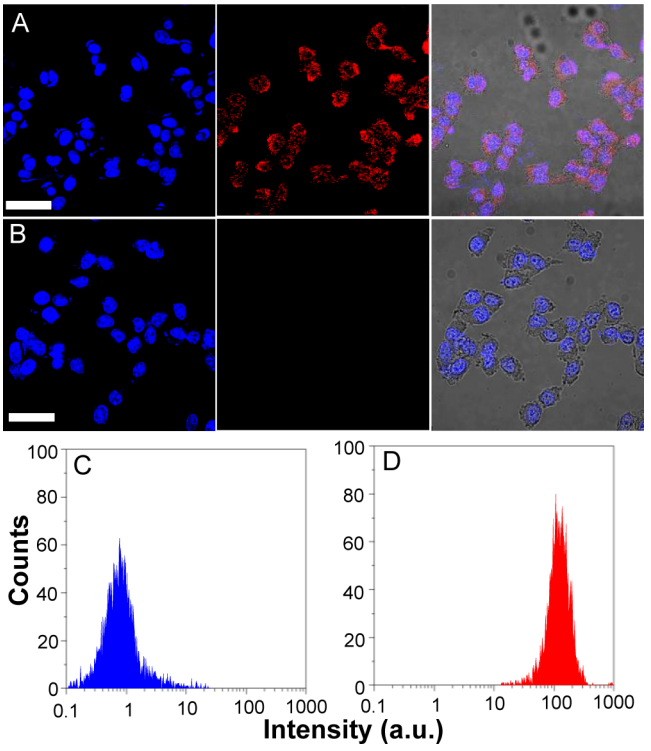

Figure 5. Two-color confocal fluorescence images of MCF-7 cells labeled with Pdot-streptavidin conjugates. (A) Blue fluorescence is from nuclear counterstain Hoechst 34580, and red fluorescence is from Pdot-streptavidin. The right panel shows fluorescence overlaid with bright-field image. (B) Images of negative control samples in which cells were incubated with Pdot-streptavidin probes but in the absence of primary biotin antihuman CD326 EpCAM antibody. The scale bars are 30 μm.

labeled onto the surfaces of MCF-7 cells, while no observable emission signal on the cell surfaces was detected for the negative control sample (Figure 5B) where primary biotin antihuman CD326 EpCAM antibody was absent. We also performed flow cytometry experiments to further evaluate the labeling efficiency of the Pdot-streptavidin probes in large scale analysis. Figure 5C−D shows the flow cytometry results in which a great separation between the Pdot-labeled cells (Figure 5C, in the presence of primary antibody) and the negative control (Figure 5D, in the absence of primary antibody) could be obviously seen. This indicates that Pdot-streptavidin conjugates can be specifically and effectively targeted onto MCF-7 cells with minimal nonspecific adsorption, which is consistent with the results observed in the confocal fluorescence images (Figure 4).

CONCLUSIONS

In summary, we have successfully developed a series of ultrabright NIR-emitting Pdots with large Stokes shifts based on dithienylbenzoselenadiazole derivatives. We found the alkyl substitution on thiophene rings in DBS plays an important role in the interchain interaction at an increased DBS concentration. These Pdots can be readily excited by a 488 nm laser or a longer wavelength (e.g., 532 nm) laser for the Pdots with DBS content higher than 10%, in which we also have demonstrated that a higher molar ratio of DBS is prerequisite to have good Pdot photostability. Single-particle brightness measurements indicate that the DBS-based Pdots are at least 2 times brighter than Qdot705. Besides, the covalent fabrication of carboxylic acid groups on the side chains of fluorene monomers offered the feasibility for further bioconjugation and sensing applications. We have demonstrated the bioconjugation of the carboxyl-functionalized Pdots and their highly specific labeling ability to both cell surfaces and interiors without any observable nonspecific adsorption. We expect this new type of DBS-based NIR-emitting Pdots to find broad use both in basic biological studies and in bioimaging and bioanalytical applications.

EXPERIMENTAL SECTION

Materials. All of the chemicals were purchased from Sigma-Aldrich or Alfa Aesar and used as received unless indicated elsewhere. All biorelated agents such as streptavidin, anitibody, or medium are purchased form Invitrogen (Life Technologies). High purity water (18.2 MΩ•cm) was used throughout the experiment. All ^{1}H NMR and ^{13}C NMR spectra were recorded on a Bruker AV400 spectrometer (400 MHz). The preparation of Pdots and the experimental procedures of cell culture and labeling have been previously reported.[53]

*Synthesis of 4,7-Dibromobenzo[C][1,2,5]thiadiazole, **1**.* Four g (29.37 mmol) of benzo[1,2,5]thiadiazole was dissolved in 30 mL of hydrobromic acid (48 wt % solution in H_2O) in a round-bottomed two-necked flask and then heated to 70 °C with stirring. 4.5 mL (87.85 mmol) of bromine was added dropwise and then stirred for 6 h under reflux. After cooling down to room temperature, the reaction mixture was pour into 100 mL of $NaHSO_3$ (0.3 M) and stirred for 30 min. The solution was then extracted with CH_2Cl_2 and sequentially washed with saturated $NaHCO_3$ and Na_2CO_3. The organic extract was separated and dried over $MgSO_4$, and the solvent was removed under reduced pressure. The product was further reprecipitated using CH_2Cl_2/methanol and then filtered to afford 6 g (69%) of **1** as a white needle-like solid. ^{1}H NMR (400 MHz, $CDCl_3$): δ = 7.71 (s, 2H).

*Synthesis of 3,6-Dibromobenzene-1,2-diamine, **2**.* Two g (6.8 mmol) of **1** was dissolved in 30 mL of ethanol in a single-necked flask and then cooled to 0 °C. Four g (0.11 mol) of sodium borohydride in 30 mL of ethanol was then added dropwise. The reaction mixture was allowed to warm up to room temperature and stirred for 40 h. After that, the solvent was removed by rotary evaporator, and then the residue was dissolved in CH_2Cl_2 to extract with brine. The organic extract was separated and dried over $MgSO_4$, and the solvent was removed under reduced pressure to obtain 1.7 g (93%) of **2** as a white solid. ^{1}H NMR (400 MHz, $CDCl_3$): δ = 6.85 (s, 2H), 3.91 (s, 4H).

*Synthesis of 4,7-Dibromobenzo[c][1,2,5]selenadiazole, **3**.*[31] 1.7 g (6.39 mmol) of **2** in 40 mL of ethanol in a round-bottomed single-necked flask was heated to reflux, and then 0.78 g (7.03 mmol) of SeO_2 in 40 mL of hot water was added. The reaction mixture was stirred and refluxed for 3 h to afford a suspension solution. After that, the reaction mixture was filtered, and the solid was washed with copious methanol and water. The product was further reprecipitated in EA/methanol and EA/hexane to yield 1.5 g (68%) of **3** as a yellow solid. ^{1}H NMR (400 MHz, $CDCl_3$): δ = 7.64 (s, 2H).

*Synthesis of Tributyl(thiophen-2-yl)stannane, **4**.*[55] A solution of 3 mL (37.44 mmol) of thiophene in 20 mL of THF was cooled to −78

°C under nitrogen atmosphere. Twenty-eight mL (44.8 mmol) of *n*-BuLi (1.6 M in hexane) was added dropwise to the solution by syringe, and the reaction mixture was allowed to warm up to room temperature and stirred for 2 h. After that, the solution was cooled to 0 °C, and 10.2 mL (37.66 mmol) of tributyltin chloride was added. After being stirred for 2 h, the mixture was poured into water, diluted with hexane, and then extracted with brine. The organic extract was separated and dried over $MgSO_4$, and the solvent was removed under reduced pressure. The residue was purified by flash column chromatography on aluminum oxide, eluting with hexane. The crude product **4** was obtained and used directly in the next step without deliberate purification.

*Synthesis of 3-Hexylthiophene, **5**.*[56] To a round-bottomed two-necked flask was added 2 g (83.33 mmol) of Mg, 25 mL of THF, and 9.4 mL (66.97 mmol) of bromohexane under a nitrogen atmosphere, and then the mixture was refluxed at 80 °C for 3 h. After cooling down to room temperature, the reaction mixture was slowly transferred to a 20 mL THF solution containing 5.2 mL (55.50 mmol) of 3-bromothiophene and 0.6 g (1.14 mmol) of [1,2-bis-(diphenylphosphino)ethane]dichloronickel(II) under nitrogen. The reaction mixture was then refluxed for 3 h and further stirred at room temperature for 12 h. After that, the reaction was quenched with HCl (l M solution) and then diluted with diethyl ether to extract with brine. The organic extract was separated and dried over $MgSO_4$, and the solvent was removed under reduced pressure. The crude product was purified by column chromatography on silica gel using hexane as eluent to yield 7 g (74%) of **5** as light yellow oil. ^{1}H NMR (400 MHz, $CDCl_3$): δ = 7.25−7.22 (m, 1H), 6.95−6.92 (m, 2H), 2.66−2.61 (t, J = 9 Hz, 2H), 1.68−1.39 (m, 2H), 1.63−1.44 (m, 4H), 0.92−0.87 (t, J = 9 Hz, 3H).

*Synthesis of Tributyl(4-hexylthiophen-2-yl)stannane, **6**.*[56] A solution of 1 mL (5.56 mmol) of **5** in 20 mL of THF was cooled to −78 °C under nitrogen atmosphere. 4.2 mL (6.72 mmol) of *n*-BuLi (1.6 M in hexane) was added dropwise to the solution, and the reaction mixture was allowed to warm up to room temperature and stirred for 2 h. After that, the solution was cooled to 0 °C, and 1.6 mL (5.90 mmol) of tributyltin chloride was added. After being stirred for 2 h, the mixture was poured into water, and diluted with hexane to extract with brine. The organic extract was separated and dried over $MgSO_4$, and the solvent was removed under reduced pressure. The crude product was purified by flash column chromatography on aluminum oxide, eluting with hexane to obtain product **6** a yellow oil. The crude product was used directly in the next step.

*Synthesis of 4,7-Di(thiophen-2-yl)benzo[c][1,2,5]selenadiazole, **7a**.*[56] To a round-bottomed two-necked flask was added 0.4 g (0.57 mmol) of $Pd(PPh_3)_2Cl_2$ and 1.4 g (4.11 mmol) of **3**. The flask was degassed and refilled with nitrogen, and then 35 mL of THF and 3.4 g (9.11 mmol) of **4** was added. The reaction mixture was refluxed at 80 °C under nitrogen for 24 h. After the reaction, 10 mL of hexane and silica gel was added, and then the solvent was removed by a rotary evaporator for column chromatography. The crude product was purified by column chromatography on a silica gel, eluting with 1:5 (v/v) of CH_2Cl_2/hexane to yield 380 mg (26%) of the **7a** as a red solid. ^{1}H NMR (400 MHz, $CDCl_3$): δ = 8.03−8.02 (d, J = 3 Hz, 2H), 7.8 (s, 2H), 7.47−7.46 (d, J = 3 Hz, 2H), 7.21−7.18 (t, J = 3 Hz, 2H).

*Synthesis of 4,7-Bis(4-hexylthiophen-2-yl)benzo[c][1,2,5]-selenadiazole, **7b**.* To a round-bottomed two-necked flask was added 0.115 g (0.16 mmol) of $Pd(PPh_3)_2Cl_2$ and 0.9 g (2.64 mmol) of **3**. The flask was degassed and refilled with nitrogen, and then 35 mL of THF and 2.8 g (6.12 mmol) of **6** was added. The reaction mixture was refluxed at 80 °C under nitrogen for 24 h. After that, 10 mL of hexane and silica gel was added, and then the solvent was removed by a rotary evaporator for column chromatography. The crude product was purified by column chromatography on a silica gel, eluting with 1:5 (v/v) of CH_2Cl_2/hexane to yield 1 g (71%) of the **7b** as a red solid. ^{1}H NMR (400 MHz, $CDCl_3$): δ = 7.88 (s, 2H), 7.75 (s, 2H), 7.04 (s, 2H), 2.71−2.66 (t, J = 6 Hz, 4H), 1.72−1.42 (m, 4H), 1.40−1.33 (m, 12H), 0.93−0.88 (m,6H).

*Synthesis of 4,7-Bis(3-hexylthiophen-2-yl)benzo[c][1,2,5]-selenadiazole, **7c**.* To a round-bottomed two-necked flask, 200 mg (0.68 mmol) of 2-(3-hexylthiophen-2-yl)-4,4,5,5-tetramethyl-1,3,2-dioxaborolane and 104 mg (0.31 mmol) of **3** were dissolved in 9 mL of toluene, and then 6 mL of ethanol and 20 mL of Na_2CO_3 (2 M) were added. The mixture solution was purged with nitrogen for 1 h, and then the mixture was degassed and refilled with N_2 (repeated 4 times) before and after addition of $Pd(PPh_3)_4$ (18 mg, 0.016 mmol). The reaction mixture was reflux under nitrogen for 48 h. After that, the solvent was removed by a rotary evaporator and diluted with CH_2Cl_2 to extract with brine. The organic extract was separated and dried over $MgSO_4$, and the solvent was removed under reduced pressure. The crude product was purified by column chromatography on silica gel, eluting with CH_2Cl_2/hexane to yield 139 mg (85%) of **7c** as orange oil. ^{1}H NMR (400 MHz, $CDCl_3$): δ = 7.52 (s, 2H), 7.43−7.41 (d, J = 6 Hz, 4H), 7.09−7.08 (d, J = 3 Hz, 4H), 2.66−2.61 (t, J = 6 Hz, 4H), 1.65−1.58 (m, 4H), 1.24−1.20 (m, 12H), 0.83−0.79 (m, 6H).

*Synthesis of 4,7-Bis(5-bromothiophen-2-yl)benzo[c][1,2,5]-selenadiazole, **8a**.*[56] 380 mg (1.09 mmol) of **7a** was dissolved in 9 mL of chloroform and 9 mL of acetic acid in a round-bottomed single-necked flask and then cooled to 0 °C. 400 mg (2.24 mmol) of *n*-bromosuccinimide (NBS) solid was then added in one portion. After being stirred in the dark at room temperature for 11 h as a suspension solution, the reaction mixture was filtered and washed several times with methanol and water to afford 250 mg (45%) of **8a** as a deep red solid. MALDI MS: m/z 505.7 (M^+). ^{1}H NMR (400 MHz, $CDCl_3$): δ = 7.73 (s, 2H), 7.71−7.70 (d, J = 3 Hz, 2H), 7.14−7.13 (d, J = 3 Hz, 2H).

*Synthesis of 4,7-Bis(5-bromo-4-hexylthiophen-2-yl)benzo[c]-[1,2,5]selenadiazole, **8b**.* One g (1.89 mmol) of **7b** was dissolved in 30 mL of DMF in a round-bottomed single-necked flask and cooled to 0 °C. 0.7 g (3.93 mmol) of *n*-bromosuccinimide (NBS) dissolved in 10 mL of DMF was added dropwise to the solution via a dropping funnel. After being stirred in the dark at room temperature for 11 h, the reaction mixture was pour into water, diluted with CH_2Cl_2, and extracted with brine. The organic extract was separated and dried over $MgSO_4$, and the solvent was removed under reduced pressure. The crude product was purified on a silica gel column, by eluting with hexane to yield 1 g (76%) of **8b** as a deep red solid. MALDI MS: m/z 674.0 (M^+). ^{1}H NMR (400 MHz, $CDCl_3$): δ = 7.70 (s, 2H), 7.66 (s, 2H), 2.66−2.61 (t, J = 6 Hz, 4H), 1.67−1.64 (m, 4H), 1.35−1.26 (m, 12H), 0.93−0.88 (t, J = 9 Hz, 6H). ^{13}C NMR (400 MHz, $CDCl_3$): δ = 157.73, 142.64, 138.77, 127.67, 126.73, 124.97, 112.23, 31.65, 29.76, 29.67, 28.98, 22.62, 14.10.

*Synthesis of 4,7-Bis(5-bromo-3-hexylthiophen-2-yl)benzo[c]-[1,2,5]selenadiazole, **8c**.* 139 mg (0.26 mmol) of **7c** was dissolved in 10 mL of DMF in a round-bottomed single-necked flask and cooled to 0 °C. 98 mg (0.55 mmol) of *n*-bromosuccinimide (NBS) dissolved in 3 mL of DMF was added dropwise to the solution via a dropping funnel. After being stirred in the dark at room temperature for 12 h, the reaction mixture was pour into water, diluted with hexane, and extracted with brine for 3 times. The organic extract was separated and dried over $MgSO_4$, and the solvent was removed under reduced pressure. The crude product was purified on a silica gel column, by eluting with hexane to yield 136 mg (77%) of **8c** as a red solid. MALDI MS: m/z 674.9 (M^+). ^{1}H NMR (400 MHz, $CDCl_3$): δ = 7.48 (s, 2H), 7.04 (s, 2H), 2.61−2.56 (t, J = 6 Hz, 4H), 1.59−1.59 (m, 4H), 1.25−1.20 (m, 12H), 0.81 (m, 6H). ^{13}C NMR (400 MHz, $CDCl_3$): δ = 159.32, 142.7, 134.05, 131.81, 129.89, 128.22, 113.12, 31.52, 30.51, 29.43, 29.02, 22.51, 14.04.

General Procedures of Polymerization.[31] The Suzuki coupling reaction was used to synthesize the copolymers as shown in Scheme 1. In a 100 mL flask, monomer **1** (0 mmol−0.49 mmol), monomer **8a or 8b or 8c** (0.5 mmol-0.01 mmol), monomer **9** (0.5 mmol, see the Supporting Information for synthetic details), and monomer **12** (0−0.03 mmol) were dissolved in 20 mL of toluene, and then 6.25 mg (0.02 mmol) of tetra-*n*-butylammonium bromide (Bu_4NBr) and 6 mL of Na_2CO_3 (2 M) was added. The mixture solution was purged with nitrogen for 1 h. After that, the mixture solution was degassed and refilled with N_2 (repeated 4 times) before and after the addition of $Pd(PPh_3)_4$ (27 mg, 0.023 mmol). The reactants were stirred at 100 °C for 48 h, and then 50 mg of phenylboronic acid dissolved in 1 mL of

THF was added. After 2 h, 0.5 mL of bromobenzene was added and further stirred for 3 h. The mixture was poured into 120 mL of methanol. The precipitate was filtered, washed with methanol and acetone to remove monomers, small oligomers, and inorganic salts. The crude product was dissolved in CH_2Cl_2 and then extracted with brine for 3 times. The organic extract was separated and dried over $MgSO_4$, and the solvent was removed under reduced pressure. The crude polymers were reprecipitated in $CHCl_3$/methanol and washed with acetone. Finally, the product was collected by filtration to afford 120−150 mg of polymer **PFBT-DBSX**, **PFBT-DBSOC$_6$X**, **PFBT-DBSIC$_6$X**, **PFBT-DBSOC$_6$10-BOC**, or **PFBT-DBSOC$_6$10-COOH**. GPC: **PFBT-DBS1** M_n: 4289, M_w: 6623, PDI: 1.54, ^{1}H NMR (δ, $CDCl_3$): 0.58−0.79 (m, 6H, CH_3), 0.81−1.38 (m, 24H, CH_2), 1.88−2.15 (m, 4H), 7.32−8.12 (m, 12H); **PFBT-DBS4** M_n: 3177, M_w: 5311, PDI: 1.67, ^{1}H NMR (δ, $CDCl_3$): 0.57−0.80 (m, 6H, CH_3), 0.81−1.36 (m, 24H, CH_2), 1.75−2.15 (m, 4H), 7.32−8.12 (m, 12H); **PFBT-DBS10** M_n: 3587, M_w: 5141, PDI: 1.43; **PFBT-DBS33** M_n: 6587, M_w: 7701, PDI: 1.17, ^{1}H NMR (δ, $CDCl_3$): 0.58−0.79 (m, 6H, CH_3), 0.81−1.38 (m, 24H, CH_2), 1.88−2.15 (m, 4H), 7.32−8.12 (m, 12H); **PFBT-DBS50** M_n: 4022, M_w: 5449, PDI: 1.35, ^{1}H NMR (δ, $CDCl_3$): 0.56−0.79 (m, 6H, CH_3), 0.81−1.37 (m, 24H, CH_2), 1.86−2.15 (m, 4H), 7.32−8.10 (m, 12H); **PFBT-DBSIC$_6$1** M_n: 9266, M_w: 11202, PDI: 1.21, ^{1}H NMR (δ, $CDCl_3$): 0.69−0.95 (m, 6H, CH_3), 1.00−1.70 (m, 24H, CH_2), 1.80−2.60 (m, 4H), 2.70−2.80 (m, 1H), 7.27−8.30 (m, 6H); **PFBT-DBSIC$_6$4** M_n: 12195, M_w: 18434, PDI: 1.51, ^{1}H NMR (δ, $CDCl_3$): 0.69−0.95 (m, 6H, CH_3), 1.00−1.75 (m, 25H, CH_2), 1.80−2.30 (m, 4H), 2.60−2.80 (m, 1H), 7.27−8.30 (m, 6H); **PFBT-DBSIC$_6$10** M_n: 11131, M_w: 26238, PDI: 2.55, ^{1}H NMR (δ, $CDCl_3$): 0.69−0.95 (m, 7H, CH_3), 1.02−1.60 (m, 27H, CH_2), 1.70−2.25 (m, 4H), 2.60−2.80 (m, 1H), 7.27−8.30 (m, 6H); **PFBT-DBSIC$_6$33** M_n: 12188, M_w: 20270, PDI: 1.66, ^{1}H NMR (δ, $CDCl_3$): 0.64−0.90 (m, 10H, CH_3), 0.91−1.60 (m, 34H, CH_2), 1.70−2.30 (m, 4H), 2.52−2.89 (m, 2H), 7.27−8.30 (m, 7H); **PFBT-DBSIC$_6$50** M_n: 10857, M_w: 24454, PDI: 2.25, ^{1}H NMR (δ, $CDCl_3$): 0.64−0.90 (m, 12H, CH_3), 0.91−1.82 (m, 40H, CH_2), 1.84−2.18 (m, 4H), 2.55−2.89 (m, 4H), 7.30−7.90 (m, 10H); **PFBT-DBSOC$_6$1** M_n: 11009, M_w: 26839, PDI: 2.44, ^{1}H NMR (δ, $CDCl_3$): 0.60−0.90 (m, 6H, CH_3), 0.92−1.80 (m, 24H, CH_2), 1.82−2.2 (m, 4H), 2.60−2.90 (m, 1H), 7.30−8.10 (m, 6H); **PFBT-DBSOC$_6$4** M_n: 9711, M_w: 18607, PDI: 1.92, ^{1}H NMR (δ, $CDCl_3$): 0.59−0.85 (m, 6H, CH_3), 0.86−1.75 (m, 25H, CH_2), 1.81−2.40 (m, 4H), 2.60−2.80 (m, 1H), 7.20−8.20 (m, 6H); **PFBT-DBSOC$_6$10** M_n: 13228, M_w: 28955, PDI: 2.19, ^{1}H NMR (δ, $CDCl_3$): 0.60−0.95 (m, 7H, CH_3), 1.02−1.70 (m, 27H, CH_2), 1.73−2.25 (m, 4H), 2.60−2.80 (m, 1H), 7.27−8.32 (m, 6H); **PFBT-DBSOC$_6$33** M_n: 15033, M_w: 31636, PDI: 2.10, ^{1}H NMR (δ, $CDCl_3$): 0.54−0.84 (m, 10H, CH_3), 0.91−1.79 (m, 34H, CH_2), 1.81−2.13 (m, 4H), 2.62−2.89 (m, 2H), 7.31−8.09 (m, 7H); **PFBT-DBSOC$_6$50** M_n: 14207, M_w: 30177, PDI: 2.12, ^{1}H NMR (δ, $CDCl_3$): 0.55−0.85 (m, 12H, CH_3), 0.86−1.86 (m, 40H, CH_2), 1.90−2.16 (m, 4H), 2.66−2.98 (m, 4H), 7.35−8.12 (m, 10H); **PFBT-DBSOC$_6$10-BOC** M_n: 3646, M_w: 5671, PDI: 1.55.

Cell Imaging. The emission spectra of Pdot-labeled cells were obtained with a fluorescence confocal microscope (Nikon D-Eclipse C1) under ambient conditions (24 ± 2 °C). The images were acquired by use of a diode laser at 488 nm (~15 mW) as the excitation source and an integration time of 1.6 μs/pixel. A CF1 Plan Fluor 100× (N. A. 1.30, W.D. 0.16 mm) oil objective was employed for imaging and spectral data acquisition; the laser was focused to a spot size of ~7 μm^2. The blue fluorescence was collected by filtering through a 450/35 band-pass (λ_{ex} = 408 nm), while the red fluorescence was collected by filtering through a 570 long-pass (λ_{ex} = 488 nm).

■ ASSOCIATED CONTENT

Supporting Information

Details of synthetic procedures of PFBT-DBSOC$_5$O10, PFBT-DBSOBR10, NMR spectra, Schemes S1−S2, Table S1, and Figures S1−S2. This material is available free of charge via the Internet at http://pubs.acs.org.

■ AUTHOR INFORMATION

Corresponding Author

*E-mail: yhchan@mail.nsysu.edu.tw.

Notes

The authors declare no competing financial interest.

■ ACKNOWLEDGMENTS

We would like to thank the Ministry of Science (103-2113-M-110-004-MY2), NSYSU-KMU Joint Research Project (103-I 004), and National Sun Yat-sen University. We also gratefully acknowledge support from Prof. Chao-Ming Chiang, Prof. Wei-Lung Tseng, Prof. Chin-Hsing Chou, and Dr. Jiun-Yi Shen from National Taiwan University. We especially thank Dr. Fangmao Ye for the measurements of single-particle fluorescence brightness.

■ REFERENCES

(1) Rubinson, E. H.; Gowda, A. S. P.; Spratt, T. E.; Gold, B.; Eichman, B. F. An Unprecedented Nucleic Acid Capture Mechanism for Excision of DNA Damage. *Nature* **2010**, *468*, 406−411.

(2) Rosenfeld, N.; Young, J. W.; Alon, U.; Swain, P. S.; Elowitz, M. B. Gene Regulation at the Single-Cell Level. *Science* **2005**, *307*, 1962−1965.

(3) Kotecha, N.; Flores, N. J.; Irish, J. M.; Simonds, E. F.; Sakai, D. S.; Archambeault, S.; Diaz-Flores, E.; Coram, M.; Shannon, K. M.; Nolan, G. P.; Loh, M. L. Single-Cell Profiling Identifies Aberrant STAT5 Activation in Myeloid Malignancies with Specific Clinical and Biologic Correlates. *Cancer Cell* **2008**, *14*, 335−343.

(4) Frangioni, J. V. New Technologies for Human Cancer Imaging. *J. Clin. Oncol.* **2008**, *26*, 4012−4021.

(5) Dam, G. M. v.; Themelis, G.; Crane, L. M. A.; Harlaar, N. J.; Pleijhuis, R. G.; Kelder, W.; Sarantopoulos, A.; Jong, J. S. d.; Arts, H. J. G.; Zee, A. G. J. v. d.; Bart, J.; Low, P. S.; Ntziachristos, V. Intraoperative Tumor-Specific Fluorescence Imaging in Ovarian Cancer by Folate Receptor-α Targeting: First in-Human Results. *Nat. Med.* **2011**, *17*, 1315−1319.

(6) Jin, Y.; Ye, F.; Zeigler, M.; Wu, C.; Chiu, D. T. Near-Infrared Fluorescent Dye-Doped Semiconducting Polymer Dots. *ACS Nano* **2011**, *5*, 1468−1475.

(7) Yuan, L.; Lin, W.; Zhao, S.; Gao, W.; Chen, B.; He, L.; Zhu, S. A Unique Approach to Development of Near-Infrared Fluorescent Sensors for in Vivo Imaging. *J. Am. Chem. Soc.* **2012**, *134*, 13510−13523.

(8) Medintz, I. L.; Uyeda, H. T.; Goldman, E. R.; Mattoussi, H. Quantum Dot Bioconjugates for Imaging, Labelling and Sensing. *Nat. Mater.* **2005**, *4*, 435−446.

(9) Somers, R. C.; Bawendi, M. G.; Nocera, D. G. CdSe Nanocrystal Based Chem-/Bio- Sensors. *Chem. Soc. Rev.* **2007**, *36*, 579−591.

(10) Choi, H. S.; Liu, W.; Misra, P.; Tanaka, E.; Zimmer, J. P.; Ipe, B. I.; Bawendi, M. G.; Frangioni, J. V. Renal Clearance of Quantum Dots. *Nat. Biotechnol.* **2007**, *25*, 1165−1170.

(11) Michalet, X.; Pinaud, F. F.; Bentolila, L. A.; Tsay, J. M.; Doose, S.; Li, J. J.; Sundaresan, G.; Wu, A. M.; Gambhir, S. S.; Weiss, S. Quantum Dots for Live Cells, in Vivo Imaging, and Diagnostics. *Science* **2005**, *307*, 538−544.

(12) Derfus, A. M.; Chan, W. C. W.; Bhatia, S. N. Probing the Cytotoxicity of Semiconductor Quantum Dots. *Nano Lett.* **2004**, *4*, 11−18.

(13) Bae, S. W.; Tan, W.; Hong, J.-I. Fluorescent Dye-Doped Silica Nanoparticles: New Tools for Bioapplications. *Chem. Commun.* **2012**, *48*, 2270−2282.

(14) Yan, J.; Estéveza, M. C.; Smith, J. E.; Wang, K.; He, X.; Wang, L.; Tan, W. Dye-Doped Nanoparticles for Bioanalysis. *Nano Today* **2007**, *2*, 44−50.

(15) Lee, J. E.; Lee, N.; Kim, H.; Kim, J.; Choi, S. H.; Kim, J. H.; Kim, T.; Song, I. C.; Park, S. P.; Moon, W. K.; Hyeon, T. Uniform Mesoporous Dye-Doped Silica Nanoparticles Decorated with Multiple

Magnetite Nanocrystals for Simultaneous Enhanced Magnetic Resonance Imaging, Fluorescence Imaging, and Drug Delivery. *J. Am. Chem. Soc.* **2010**, *132*, 552−557.
(16) Reul, R.; Tsapis, N.; Hillaireau, H.; Sancey, L.; Mura, S.; Recher, M.; Nicolas, J.; Collcd, J.-L.; Fattal, E. Near Infrared Labeling of PLGA for In Vivo Imaging of Nanoparticles. *Polym. Chem.* **2012**, *3*, 694−702.
(17) Yang, Y.; An, F.; Liu, Z.; Zhang, X.; Zhou, M.; Li, W.; Hao, X.; Lee, C.-s.; Zhang, X. Ultrabright and Ultrastable Near-Infrared Dye Nanoparticles for In Vitro and In Vivo Bioimaging. *Biomaterials* **2012**, *33*, 7803−7809.
(18) Peng, J.; He, X.; Wang, K.; Tan, W.; Wang, Y.; Liu, Y. Noninvasive Monitoring of Intracellular pH Change Induced by Drug Stimulation Using Silica Nanoparticle Sensors. *Anal. Bioanal. Chem.* **2007**, *388*, 645−654.
(19) Peng, H.-s.; Stolwijk, J. A.; Sun, L.-N.; Wegener, J.; Wolfbeis, O. S. A Nanogel for Ratiometric Fluorescent Sensing of Intracellular pH Values. *Angew. Chem., Int. Ed.* **2010**, *49*, 4246−4249.
(20) Brunetti, V.; Chibli, H.; Fiammengo, R.; Galeone, A.; Malvindi, M. A.; Vecchio, G.; Cingolani, R.; Nadeau, J. L.; Pompa, P. P. InP/ZnS as a Safer Alternative to CdSe/ZnS Core/Shell Quantum Dots: In Vitro and In Vivo Toxicity Assessment. *Nanoscale* **2013**, *5*, 307−317.
(21) Tsoi, K. M.; Dai, Q.; Alman, B. A.; Chan, W. C. W. Are Quantum Dots Toxic? Exploring the Discrepancy Between Cell Culture and Animal Studies. *Acc. Chem. Res.* **2013**, *46*, 662−671.
(22) Mader, H. S.; Kele, P.; Saleh, S. M.; Wolfbeis, O. S. Upconverting Luminescent Nanoparticles for Use in Bioconjugation and Bioimaging. *Curr. Opin. Chem. Biol.* **2010**, *14*, 582−596.
(23) Wu, C.; Bull, B.; Szymanski, C.; Christensen, K.; McNeill, J. Multicolor Conjugated Polymer Dots for Biological Fluorescence Imaging. *ACS Nano* **2008**, *2*, 2415−2423.
(24) Tian, Z.; Yu, J.; Wu, C.; Szymanski, C.; McNeill, J. Amplified Energy Transfer in Conjugated Polymer Nanoparticle Tags and Sensors. *Nanoscale* **2010**, *2*, 1999−2011.
(25) Pecher, J.; Mecking, S. Nanoparticles of Conjugated Polymers. *Chem. Rev.* **2010**, *110*, 6260−6279.
(26) Kaeser, A.; Schenning, A. P. H. J. Fluorescent Nanoparticles Based on Self-Assembled π-Conjugated Systems. *Adv. Mater.* **2010**, *22*, 2985−2997.
(27) Tuncel, D.; Demir, H. V. Conjugated Polymer Nanoparticles. *Nanoscale* **2010**, *2*, 484−494.
(28) Li, K.; Liu, B. Polymer Encapsulated Conjugated Polymer Nanoparticles for Fluorescence Bioimaging. *J. Mater. Chem.* **2012**, *22*, 1257−1264.
(29) Pu, K.-Y.; Liu, B. Fluorescent Conjugated Polyelectrolytes for Bioimaging. *Adv. Funct. Mater.* **2011**, *21*, 3408−3423.
(30) Wu, C.; Chiu, D. T. Highly Fluorescent Semiconducting Polymer Dots for Biology and Medicine. *Angew. Chem., Int. Ed.* **2013**, *52*, 3086−3109.
(31) Chen, C.-P.; Wu, P.-J.; Liou, S.-Y.; Chan, Y.-H. Ultrabright Benzoselenadiazole-Based Semiconducting Polymer Dots for Specific Cellular Imaging. *RSC Adv.* **2013**, *3*, 17507−17514.
(32) Chan, Y.-H.; Wu, P.-J. Semiconducting Polymer Nanoparticles as Fluorescent Probes for Biological Imaging and Sensing. *Part. Part. Syst. Charact.* **2014**, DOI: 10.1002/ppsc.201400123.
(33) Wu, C.; Jin, Y.; Schneider, T.; Burnham, D. R.; Smith, P. B.; Chiu, D. T. Ultrabright and Bioorthogonal Labeling of Cellular Targets Using Semiconducting Polymer Dots and Click Chemistry. *Angew. Chem., Int. Ed.* **2010**, *49*, 9436−9440.
(34) Wu, C.; Schneider, T.; Zeigler, M.; Yu, J.; Schiro, P. G.; Burnham, D. R.; McNeill, J. D.; Chiu, D. T. Bioconjugation of Ultrabright Semiconducting Polymer Dots for Specific Cellular Targeting. *J. Am. Chem. Soc.* **2010**, *132*, 15410−15417.
(35) Wu, C.; Hansen, S. J.; Hou, P. Q.; Yu, J.; Zeigler, M.; Jin, Y.; Burnham, D. R.; McNeill, J. D.; Olson, J. M.; Chiu, D. T. Design of Highly Emissive Polymer Dot Bioconjugates for In Vivo Tumor Targeting. *Angew. Chem., Int. Ed.* **2011**, *50*, 3430−3434.
(36) Chan, Y.-H.; Wu, C.; Ye, F.; Jin, Y.; Smith, P. B.; Chiu, D. T. Development of Ultrabright Semiconducting Polymer Dots for Ratiometric pH Sensing. *Anal. Chem.* **2011**, *83*, 1448−1455.
(37) Chan, Y.-H.; Jin, Y.; Wu, C.; Chiu, D. T. Copper(II) and Iron(II) Ion Sensing with Semiconducting Polymer Dots. *Chem. Commun.* **2011**, *47*, 2820−2822.
(38) Ye, F.; Wu, C.; Jin, Y.; Chan, Y.-H.; Zhang, X.; Chiu, D. T. Ratiometric Temperature Sensing with Semiconducting Polymer Dots. *J. Am. Chem. Soc.* **2011**, *133*, 8146−8149.
(39) Harbron, E. J.; Davis, C. M.; Campbell, J. K.; Allred, R. M.; Kovary, M. T.; Economou, N. J. Photochromic Dye-Doped Conjugated Polymer Nanoparticles: Photomodulated Emission and Nanoenvironmental Characterization. *J. Phys. Chem. C* **2009**, *113*, 13707−13714.
(40) Yu, J.; Wu, C.; Zhang, X.; Ye, F.; Gallina, M. E.; Rong, Y.; Wu, I.-C.; Sun, W.; Chan, Y.-H.; Chiu, D. T. Stable Functionalization of Small Semiconducting Polymer Dots via Covalent Cross-Linking and Their Application for Specific Cellular Imaging. *Adv. Mater.* **2012**, *24*, 3498−3504.
(41) Chan, Y.-H.; Gallina, M. E.; Zhang, X.; Wu, I.-C.; Jin, Y.; Sun, W.; Chiu, D. T. Reversible Photoswitching of Spiropyran-Conjugated Semiconducting Polymer Dots. *Anal. Chem.* **2012**, *84*, 9431−9438.
(42) Chan, Y.-H.; Ye, F.; Gallina, M. E.; Zhang, X.; Jin, Y.; Wu, I.-C.; Chiu, D. T. Hybrid Semiconducting Polymer Dot−Quantum Dot with Narrow-Band Emission, Near-Infrared Fluorescence, and High Brightness. *J. Am. Chem. Soc.* **2012**, *134*, 7309−7312.
(43) Sun, W.; Hayden, S.; Jin, Y.; Rong, Y.; Yu, J.; Ye, F.; Chan, Y.-H.; Zeigler, M.; Wu, C.; Chiu, D. T. A Versatile Method for Generating Semiconducting Polymer Dot Nanocomposites. *Nanoscale* **2012**, *4*, 7246−7249.
(44) Wu, P.-J.; Chen, J.-L.; Chen, C.-P.; Chan, Y.-H. Photoactivated Ratiometric Copper(II) Ion Sensing with Semiconducting Polymer Dots. *Chem. Commun.* **2013**, *49*, 898−900.
(45) Li, Q.; Sun, K.; Chang, K.; Yu, J.; Chiu, D. T.; Wu, C.; Qin, W. Ratiometric Luminescent Detection of Bacterial Spores with Terbium Chelated Semiconducting Polymer Dots. *Anal. Chem.* **2013**, *85*, 9087−9091.
(46) Huang, Y.-C.; Chen, C.-P.; Wu, P.-J.; Kuo, S.-Y.; Chan, Y.-H. Coumarin Dye-Embedded Semiconducting Polymer Dots for Ratiometric Sensing of Fluoride Ions in Aqueous Solution and Bioimaging in Cells. *J. Mater. Chem. B* **2014**, *2*, 6188−6191.
(47) Massin, J.; Dayoub, W.; Mulatier, J.-C.; Aronica, C.; Bretonnière, Y.; Andraud, C. Near-Infrared Solid-State Emitters Based on Isophorone: Synthesis, Crystal Structure and Spectroscopic Properties. *Chem. Mater.* **2011**, *23*, 862−873.
(48) Parka, S.-Y.; Kubotaa, Y.; Funabikia, K.; Shirob, M.; Matsui, M. Near-Infrared Solid-State Fluorescent Naphthooxazine Dyes Attached with Bulky Dibutylamino and Perfluoroalkenyloxy Groups at 6- and 9-Positions. *Tetrahedron Lett.* **2009**, *50*, 1131−1135.
(49) Fenwick, O.; Sprafke, J. K.; Binas, J.; Kondratuk, D. V.; Stasio, F. D.; Anderson, H. L.; Cacialli, F. Linear and Cyclic Porphyrin Hexamers as Near-Infrared Emitters in Organic Light-Emitting Diodes. *Nano Lett.* **2011**, *11*, 2451−2456.
(50) Qian, G.; Zhong, Z.; Luo, M.; Yu, D.; Zhang, Z.; Wang, Z. Y.; Ma, D. Simple and Efficient Near-Infrared Organic Chromophores for Light-Emitting Diodes with Single Electroluminescent Emission above 1000 nm. *Adv. Mater.* **2009**, *21*, 111−116.
(51) Lim, C.-K.; Kim, S.; Kwon, I. C.; Ahn, C.-H.; Park, S. Y. Dye-Condensed Biopolymeric Hybrids: Chromophoric Aggregation and Self-Assembly toward Fluorescent Bionanoparticles for Near Infrared Bioimaging. *Chem. Mater.* **2009**, *21*, 5819−5825.
(52) Zhang, X.; Yu, J.; Rong, Y.; Ye, F.; Chiu, D. T.; Uvdal, K. High-Intensity Near-IR Fluorescence in Semiconducting Polymer Dots Achieved by Cascade FRET Strategy. *Chem. Sci.* **2013**, *4*, 2143−2151.
(53) Wu, P.-J.; Kuo, S.-Y.; Huang, Y.-C.; Chen, C.-P.; Chan, Y.-H. Polydiacetylene-Enclosed Near-Infrared Fluorescent Semiconducting Polymer Dots for Bioimaging and Sensing. *Anal. Chem.* **2014**, *86*, 4831−4839.
(54) Zhang, X.; Yu, J.; Wu, C.; Jin, Y.; Rong, Y.; Ye, F.; Chiu, D. T. Importance of Having Low-Density Functional Groups for Generating High-Performance Semiconducting Polymer Dots. *ACS Nano* **2012**, *6*, 5429−5439.

(55) Hou, Q.; Xu, Y.; Yang, W.; Yuan, M.; Peng, J.; Gao, Y. Novel Red-Emitting Fluorene-Based Copolymers. *J. Mater. Chem.* **2002**, *12*, 2887−2892.
(56) Hou, Q.; Zhou, Q.; Zhang, Y.; Yang, W.; Yang, R.; Gao, Y. Synthesis and Electroluminescent Properties of High-Efficiency Saturated Red Emitter Based on Copolymers from Fluorene and 4,7-Di(4-hexylthien-2-yl)-2,1,3-benzothiadiazole. *Macromolecules* **2004**, *37*, 6299−6305.